Polymer Degradation and Stability 98 (2013) 2609–2616

Contents lists available at ScienceDirect

Polymer Degradation and Stability

journal homepage: www.elsevier.com/locate/polydegstab

# Nanoengineering core/shell structured brucite@polyphosphate@amine hybrid system for enhanced flame retardant properties

Xuesong Wang, Hongchang Pang, Wendan Chen, Yuan Lin, Guiling Ning*

*Faculty of Chemical, Environmental & Biological Science and Technology, Dalian University of Technology, Dalian 116024, China*

ARTICLE INFO

*Article history:*
Received 12 June 2013
Received in revised form
7 September 2013
Accepted 23 September 2013
Available online 1 October 2013

*Keywords:*
Brucite
Core/shell structure
Flame retardant
Ethylene-vinyl acetate copolymer
Mechanism

ABSTRACT

A novel organic-inorganic hybrid flame retardant consisting of a brucite core and a dodecylamine polyphosphate shell was synthesized by a facile nanoengineering route. The flammability characterization and synergistic flame retardant mechanism of the core/shell flame retardant (CFR) in ethylene-vinyl acetate (EVA) blends had been compared with EVA/physical mixture (PM, with the given proportion of brucite and dodecylamine polyphosphate as well as CFR) and EVA/brucite blends. With the same loading amount (40 wt%) of fillers in EVA, the peak heat release rate and smoke production rate of EVA/CFR blends were significantly reduced to 49% and 48% of that of EVA/PM blends, respectively. Meanwhile, the limiting oxygen index (LOI) was increased up to 32 (14.3% higher than that of EVA/PM blends) and the UL-94 test could achieve the V-0 rating. These remarkable properties were obtained just by nanoengineeing the core/shell structured brucite@polyphosphate@amine hybrid system, facilitating the formation of intact and compact residue with fence structure in process of polymer composite burning.



## 1. Introduction

Mineral fillers like brucite have been of increasing interest as halogen-free flame retardants for polymers because of its smoke suppression property, flame retardancy and good thermal stability which allows higher processing temperature [1–3]. In general, more than 60% loading amount is necessary to meet flame retardant requirements in polymer matrix [4,5]. But high filling amount of brucite is detrimental to the mechanical properties of polymer composites. Great efforts have been made on brucite incorporated with other synergistic agents [6–14] to enhance the flame resistance and improve the mechanical properties of flame retardant polymers [15]. However, most of those synergistic effects are based on simple physical mixing of brucite and synergistic agents, which still need a high loading amount of flame retardants in polymers to meet the flame retardant requirements. Although some core/shell structured flame retardants are developed as fillers in polymer composites, their flame retardant performance has not been improved significantly yet due to the unchanged mechanism of flame retarding. For example, the rheological and mechanical properties can be improved by using polystyrene-encapsulated brucite (or silane coupling agent coated brucite), which is attributed to a better dispersion and a strong adhesion between the fillers and matrix. But the flame retardant efficiency is slightly improved comparing to untreated brucite [16,17]. Moreover, other flame retardants (including red phosphorus, organic phosphate and ammonium salt) modified by coating different resins, which solve the processing and safety problem, have done nothing to help the high flame retardance or innovation of flame retarding mechanism [18–23]. To the best of our knowledge, no work has been reported on the core/shell hybrid structure involving mineral flame retardants and synergistic agent to highly decrease the necessary loading amount and significantly enhance the flame retardant efficiency.

In our previous works, we found that polyphosphate had flame retardant synergism with brucite [24]. In order to enhance the flame retarding efficiency of such composite system in polymers, we developed a hybrid structure of brucite as the core, dodecylamine polyphosphate as the shell by chemical attachment via a two-step grafting (so-called nanoengineering) route (illustrated in Scheme 1). Dodecylamine polyphosphate was used not only a synergistic agent, but also a structural stabilizer to help flame retardant particles disperse in polymer matrix (here we chose EVA) and enhance the flame retardant efficiency. In the case of lower addition of 40 wt%, the as-prepared EVA composite presented better flame resistance than conventional ones. At the initial

* Corresponding author. Tel./fax: +86 411 84986067.
*E-mail address:* ninggl@dlut.edu.cn (G. Ning).

0141-3910/$ – see front matter © 2013 Elsevier Ltd. All rights reserved.
http://dx.doi.org/10.1016/j.polymdegradstab.2013.09.021

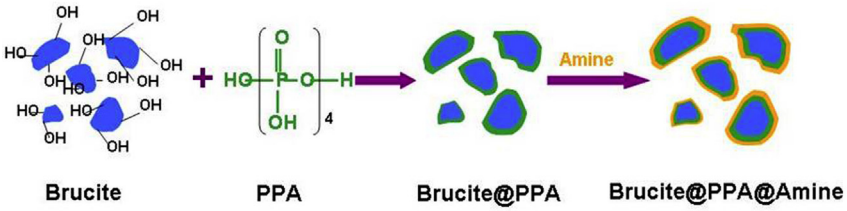


**Scheme 1.** A schematic illustration of the fabrication of CFR particles.

burning stage of the EVA composite, a large amount of intact and stable fence structures originated from highly dispersed core/shell flame retardant (CFR) particles were formed at the fire surface of the composite. The external heat radiation from burning area to the undegraded EVA was reflected and the escape of combustible gases was slowed down in the fence structures. Without enough supplement of combustible gases in burning area, the combustion was difficult to maintain. The first part of this paper concerned the evaluation of the CFR particles. In the second part, the study focused on flame retardant performances of the EVA matrix composite materials for a reasonable mechanism of flame retarding.

## 2. Experimental section

### 2.1. Materials

Brucite powder (2500 mesh) was a commercial product from Fengcheng in China. The chemical components were given in Table 1. The additives in this study were all of analytical grade (Sinopharm Chemical Reagent Co., Ltd., without any further treatment). Ethanol was industrial grade and supplied by Shandong Jinling Group Co., Ltd. EVA (7350M, Formosa Plastics Corporation) contains 18% of vinyl acetate.

### 2.2. Preparation of core/shell flame retardant (CFR) particles

The synthesis of CFR particles was illustrated in Scheme 1. In detail, 100 g of brucite was suspended in 600 mL industrial grade ethanol with refluxing for 1 h. Then 31.5 g of polyphosphoric acid (PPA) was added into the slurry slowly with the help of injection sampler at 70 °C for 10 min. Next, 9 g of dodecylamine was feed into the reaction system containing 200 mL ethanol for more than 15 min until the pH value reached to 8. Vigorous stirring was applied during the whole procedure. The product was collected and washed with ethanol several times and then Soxhlet extracted for 72 h with ethanol to remove all the physically adsorbed dodecylamine polyphosphate on the surface of CFR particles. The residues were then dried in a vacuum system at 50 °C for 6 h and the filtrate could be recycled many times.

### 2.3. Preparation of the physical mixture

For comparison, the physical mixture (PM) was prepared by mixing brucite powder and dodecylamine polyphosphate with high-speed mixer at room temperature. The dodecylamine polyphosphate was obtained using a similar synthesis method of the core/shell structural composite particles in the absence of brucite powder. The weight content of brucite in the mixture was 71.4% as well as the CFR.

**Table 1**
Chemical components of pristine brucite.

| $Mg(OH)_2$ (wt%) | $SiO_2$ (wt%) | CaO (wt%) | $Fe_2O_3$ (wt%) | Insoluble Residues (wt%) |
|---|---|---|---|---|
| ≥95 | <2 | <2 | <0.5 | <1.5 |

### 2.4. Preparation of EVA/flame retardants (FR) composites

The EVA/FR composites were prepared by melt mixing at 135 °C in an open mill for 15 min. After mixing, sheets with 4, 3 and 1 mm thickness were obtained by compression moulding under a pressure of 10 MPa at 150 °C for 10 min, respectively. The content of additives was varied from 0 to 60 wt%. Table 2 listed the EVA/FR composites of three different additives with the addition of 40 wt% for Cone Calorimeter test in this paper.

### 2.5. Characterization of powder samples

The phase structural identification of the powder samples was characterized by powder X-ray diffraction (XRD) on a Rigaku D/max 2400 X-ray diffractometer equipped with graphite monochromatized Cu Kα radiation ($\lambda$ = 1.5406 Å. The scan rate of $0.02°s^{-1}$ was applied to record the pattern in the 2θ range from 5° to 80°). Infrared spectra (IR) were recorded on a JASCO FT/IR-460 plus spectrometer using KBr disc method. The particles were gold-sputtered and morphology was measured by field emission scanning electron microscopy (FESEM) at Electron Microscope Lab, Dalian University of Technology.

The cryogenic fractured cross-sections of EVA/FR composites were obtained by liquid nitrogen (−196 °C) quenching. And part of them was etched with hydrochloric acid for 2 h to remove the surface inorganic particles. All the cryogenic fractured cross-sections were coated by gold and then the images were obtained on scanning electron microscope (SEM) (HITACHI, −4800 s) with an accelerating voltage of 20 kV.

### 2.6. Fire reaction properties of EVA/FR composites

Limiting oxygen index (LOI, Standard Test Method for measuring the minimum oxygen concentration to support candle-like downward flame combustion) was detected using an OJN - 9307 type oxygen index apparatus (Shenzhen Test Machine Co., Ltd., Guangdong Province, China) on the specimens of 120 × 6.5 × 3 $mm^3$ according to GB/T 2406-2008.

The UL-94 vertical burning tests were carried out using a M607B type instrument (Qingdao Shanfang Instrument Co., Ltd., Shandong Province, China) on the specimens of 127 × 12.7 × 3 $mm^3$ according to GB/T 2408-2008.

**Table 2**
Compositions of EVA/FR blends.

| Sample code | Formulations (wt) | Additive content (wt%) |
|---|---|---|
| A1 | EVA/brucite = 60/40 | 40 |
| A2 | EVA/PM = 60/40 | 40 |
| A3 | EVA/CFR = 60/40 | 40 |

The Cone Calorimeter (Fire Test Technology, UK) was used to test the fire behaviour of EVA/FR composites under 35 kW/m$^2$ external radiant heat flux conforming to ISO 5660 standard. A 100 × 100 × 4 mm$^3$ sheet was exposed to a radiant cone (CONE). Heat release rate (HRR), total heat evolved (THE), smoke production rate (SPR), mass loss and other parameters were recorded simultaneously. HRR was calculated as a function of the oxygen consumption linked to the combustion of the specimen using an oxygen analyser [25]. The mean HRR is usually thought to much more correlate with the heat release in room burn conditions [26,27]. As for SPR, the average values of the real-time smoke quantity were used to evaluate smoke production. Furthermore, mass loss of CONE combustion residues was calculated to corroborate their structure.

In order to easily get the SEM images of CONE combustion residues, we used alternatives that 3 × 3 × 4 mm$^3$ sheets in 3 × 3 × 5 mm$^3$ tin-foil boxes without cap were exposed to CONE in the same condition. The residues were measured by FESEM at Electron Microscope Lab, Dalian University of Technology.

## 3. Results and discussion

### 3.1. Chemical compositions and core/shell structure

FESEM and TEM images of pristine brucite and core/shell flame retardant (CFR) particles were shown in Fig. 1. In the low magnification views (Fig. 1a and b), numerous particles with micronmeter and nanometre sized diameter were observed. High magnified images shown in Fig. 1c and d suggested that surface morphologies of pristine brucite and CFR particles were of great difference. Fig. 1c revealed that pristine brucite particles had sharp angularities with comminution of brucite ore and Fig. 1d showed the different surface morphology. TEM image (Fig. 1e) showed that there was a flocculent layer on the surface of CFR particles, indicating that the CFR particles contained an apparent core/shell structure.

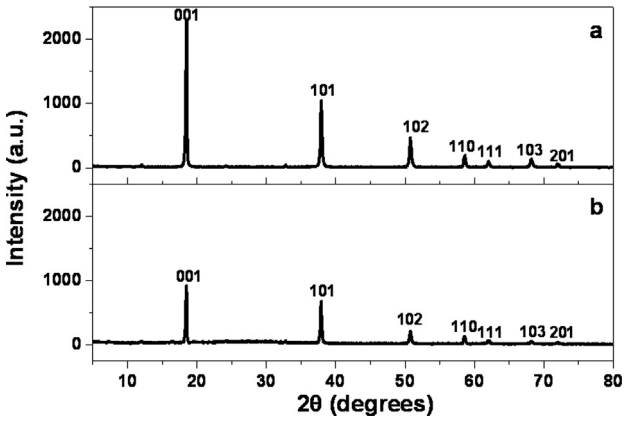


**Fig. 2.** XRD patterns for (a) pristine brucite and (b) CFR particles.

The interaction between core and shell could also be concluded from the wide angle XRD patterns, shown in Fig. 2. All diffraction peaks of each sample could be indexed as the hexagonal structure of brucite with the lattice constants comparable to the values of JCPDS 44-1482. A few unconspicuous peaks arising from impurities were detected. All of the peaks, especially the lattice plane of (001), apparently had obvious changes in intensity, suggesting that dodecylamine polyphosphate grafted on the lattice plane of (001) of burcite to form the shell structure around brucite core (shown in

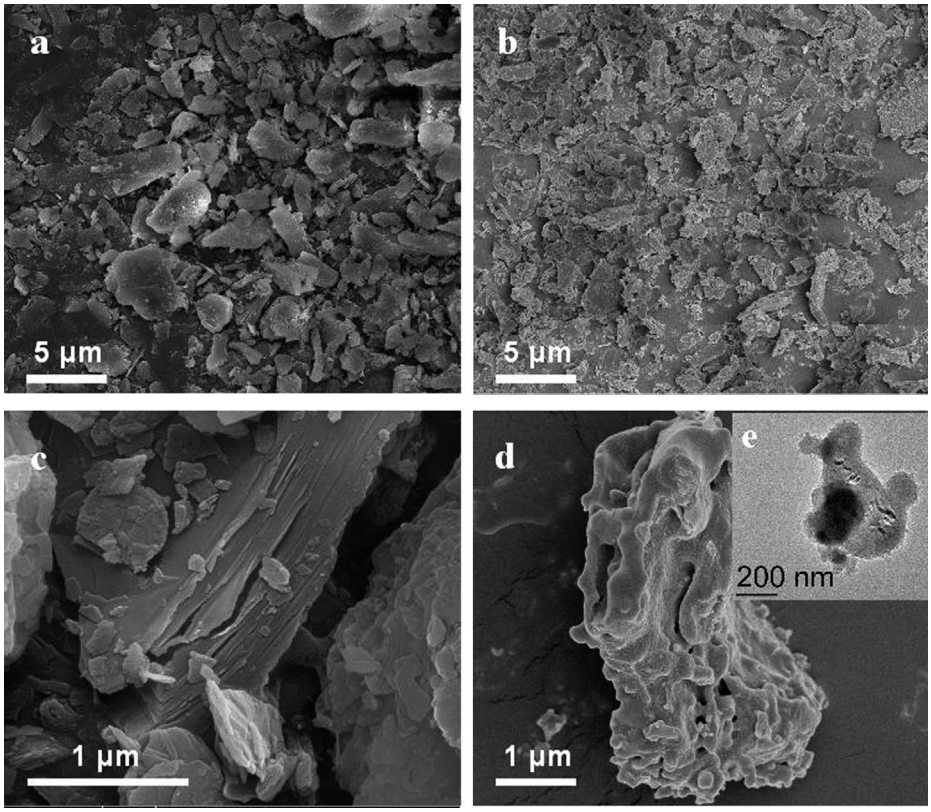


**Fig. 1.** FESEM images of (a) Low and (c) high magnification views of pristine brucite particles; (b) Low and (d) high magnification views of CFR particles. TEM images of (e) CFR particle. The core/shell structures could be observed.

Scheme 1) [28]. And the later analysis of FTIR gave more details about the formation of the core/shell structure.

In comparison with simply physical coating, we noticed that the acid–base reaction might occur between surface hydroxyl group of brucite and polyphosphoric acid (PPA). The FTIR spectra of the pristine brucite and CFR particles were shown in Fig. 3 to prove this inference. All the samples showed strong absorbances at 3694 $cm^{-1}$ and 3600 ~ 3000 $cm^{-1}$ which might be attributed to the stretching vibration bands for free and associating hydroxyl groups, respectively. Compared with pristine brucite, it was found that the stretching vibration bands of free hydroxyl group in CFR were apparently decreased at 3694 $cm^{-1}$ due to the reaction between surface free hydroxyl group of burcite particles and PPA [29,30]. And the broaden absorption at 3600 ~ 3000 $cm^{-1}$ was corresponding to N–H stretching mode from introduced dodecylamine even after extraction in Soxhlet for 72 h. The absorption at 2924 and 2851 $cm^{-1}$ in the CFR (Fig. 3b) was assigned to the symmetric and antisymmetric stretching vibration of the dodecyl groups since there was a large amount of dodecyl chains in the samples. Besides, the absorption at 1657 $cm^{-1}$ which might be assigned to the in-plane bending vibration of N–H provided the same evidence. Moreover, the characteristic absorption of 1439 $cm^{-1}$ (Fig. 3a) could be characterized as CO–Mg probably due to $CO_2$ chemisorbing on pristine brucite surface in air. And in comparison with that of pristine brucite, this absorption shifted to higher wavenumber of 1472 $cm^{-1}$ resulting from the substitution of PO–Mg between brucite and PPA (Fig. 3b). Absorptions of 437 $cm^{-1}$ (Fig. 3a) and 470 $cm^{-1}$ (Fig. 3b) could be assignable to Mg–O stretching vibration of pristine brucite and CFR, respectively. In addition, the peaks at 1123 $cm^{-1}$ together with a very weak signal at 938 $cm^{-1}$ (Fig. 3b) could be attributed to the P=O and P–O–Mg stretching modes. The above absorptions of the characteristic groups of CFR were quite different from the pristine brucite, which further confirmed that the CFR was a new hybrid core/shell structure. The FTIR absorption of brucite was more likely to be shielded by the coated dodecylamine polyphosphate. Meanwhile, the hydrophobic nature was introduced by the stretching of long dodecyl chains which took more advantages in dispersion in organic phase and polymer matrix (shown in Fig. 4 and Fig. S1). All these above analyses suggested that PPA was bonded to the brucite particles' surface and the lauryl amine was bonded to the PPA, as described in Scheme 1. In comparison with simply physical coating, lower loss in mechanical properties of EVA/CFR composite was presented by this kind of chemical attachment shown in Fig. S2, indicating that the CFR might be a remarkable and practical filler [31].

The cross-section SEM images obtained from the cryogenic EVA/flame retardants (FR) blends were shown in Fig. 4. The morphologies of EVA/FR composites (Fig. 4a, c and e) were quite different.

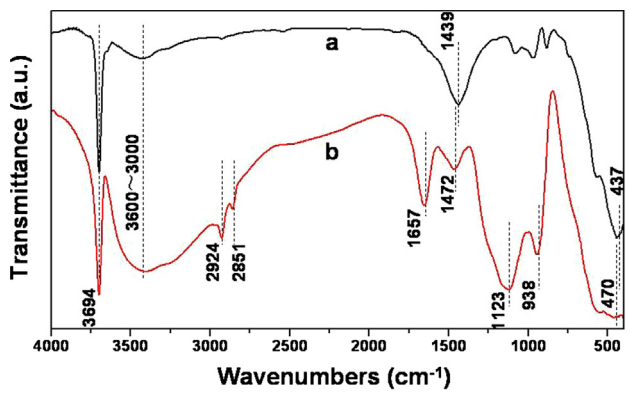


**Fig. 3.** The FTIR spectra of (a) pristine brucite particles and (b) CFR particles.

Comparing Fig. 4a with e, we could easily find that the pristine brucite particles tended to agglomerate larger ones, but the CFR particles were dispersed well in EVA matrix. After etching by hydrochloric acid, the cavities shown in Fig. 4b, d and f were clearly observed. The broad size distribution of raw brucite indicated that there existed seriously particle agglomeration which could lead to heterogeneous decomposition in fire. But the etched holes in EVA/CFR composite exhibited more uniform distribution in EVA matrix, even at the highest content of 60 wt%. Moreover, the EVA/PM composite (Fig. 4d) showed the intermediate performance with large agglomeration in comparison with EVA/brucite and EVA/CFR composites. The incorporation of dodecylamine polyphosphate chemically bonding on brucite surface could prominently improve the dispersion of CFR particles in the matrix and enhance the mechanical properties (Fig. S2). More importantly, uniform distribution of CFR particles in EVA matrix would lead to the formation of original fence structure before burning, which could prevent heat transfer and gaseous diffusion.

### 3.2. Limiting oxygen index (LOI) of EVA/FR composites

LOI and UL-94 data on different loading amount of FR particles in four kinds of formulations were listed in Table 3. It could be seen that the LOI values of EVA/FR composites were improved with increasing loading amount of any FR particles owing to the flame resistance effect of brucite and synergy dodecylamine polyphosphate. With the same addition of FR, it was obvious that the LOI values of the EVA/CFR sample were the highest. The best self-extinguishability of EVA/CFR formulation might be ascribed to the core/shell structure. In other words, this unique structure led to lower mass loss and a large amount of fence structures in combustion residue (shown in Fig. 7 and Fig. 10). Note that the LOI value of EVA/CFR composite filled with 40 wt% was still up to 32. In contrast, the corresponding formulations with EVA/brucite and EVA/PM were only 22 and 28, respectively. In addition, only the EVA/CFR composite could pass the V-0 rating of the UL-94 test. Namely, the EVA/CFR composite with addition of 40 wt% could be regarded as the fire retarding material which met the industrial standard of cable material.

### 3.3. Cone calorimeter test of EVA/FR composites

To elucidate the intrinsic reason for the enhancement of flame resistance by the core/shell structure, Cone Calorimeter test was examined [32]. The dynamic curves of heat release rate (HRR) for the samples of A1, A2 and A3 were illustrated in Fig. 5. With the same addition of FR particles, the peak intensities of A3 were much lower than any other samples apparently. It could be found that a sharp HRR peak from sample A1 appeared at the range of 120 ~ 580 s with a peak heat release rate (PHRR) of 390 $kW/m^2$, whereas sample A3 showed a dramatic decline of the HRR curve with a PHRR of 179 $kW/m^2$. The combustion time was prolonged from 470 s (A1) to 745 s (A3). The PHRR value of sample A3 was 54% lower than that of sample A1, indicating that there was remarkably synergistic action between brucite and dodecylamine polyphosphate on retard combustion. The gentle decline of HRR in samples A3 suggested that burning of the sample was gradually barriered through the formation of thick char layer (Fig. 7). This should be the reason that the residue mass loss of sample A3 was much lower than that of sample A1. Furthermore, the PHRR of sample A2 was 351 $kW/m^2$. A3 was 49% lower than this value. In this regard, the synergistic effect of core/shell structure gave the best flame retarding performance.

The dynamic curves of total heat evolved (THE) and mass loss were shown in Figs. 6 and 7, respectively. When the THE of A3 was

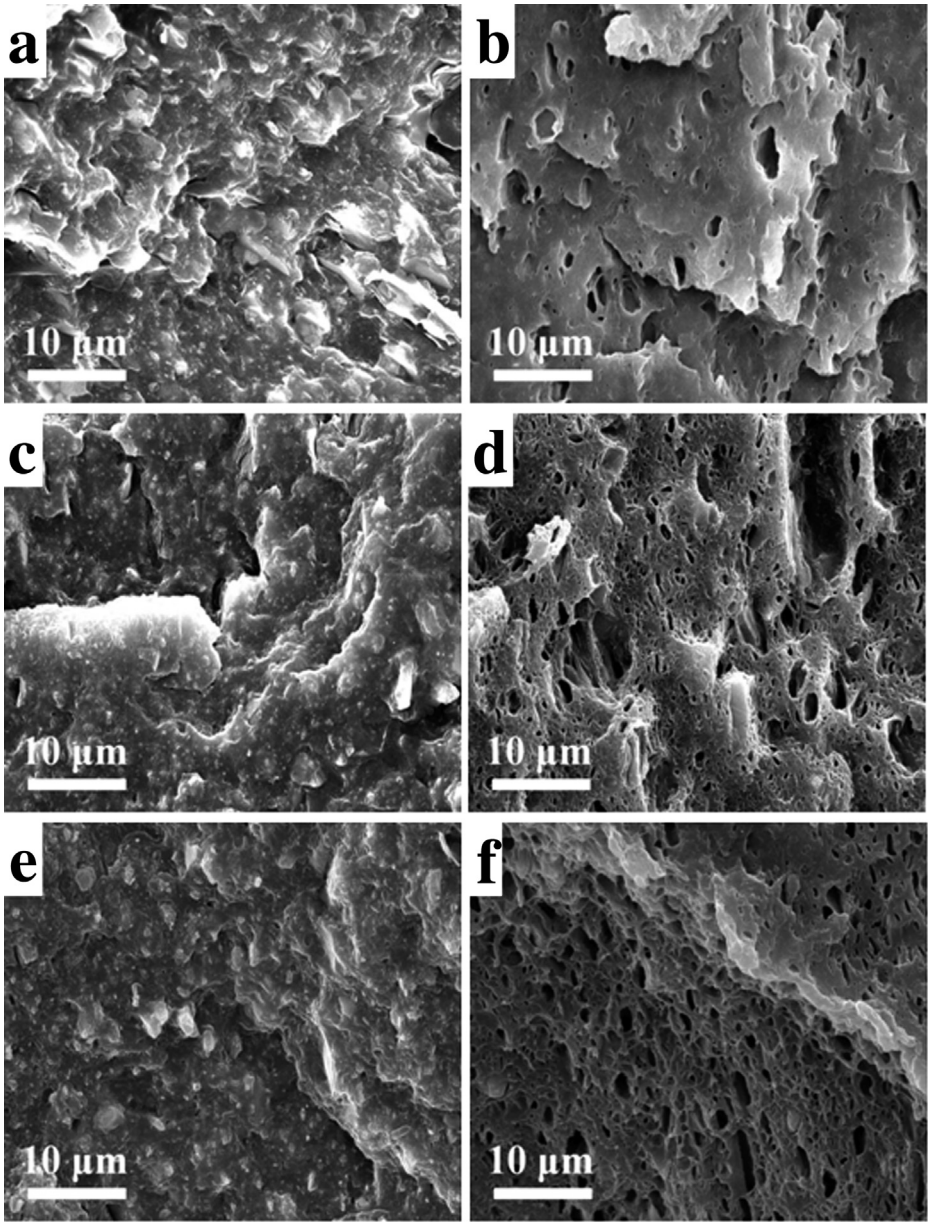


**Fig. 4.** SEM images of cryo-fracture cross-sections. (a) EVA/brucite and (b) EVA/brucite etched by hydrochloric acid. (c) EVA/PM and (d) EVA/PM etched by hydrochloric acid. (e) EVA/CFR and (f) EVA/CFR etched by hydrochloric acid. The additions of FR were all at the value of 60 wt%.

lower to the same extent with the other FR additives samples (Fig. 6), effective heat of combustion transfer could be absorbed and barriered by the condensed phase effect of the additives [33]. Interestingly, the core/shell structure also facilitated the formation of carbonaceous char in the EVA/FR composites (Fig. 7). After complete combustion in CONE, the final mass loss of A3 was 57 wt%. In contrast, A1 and A2 were 68 and 63 wt%, respectively.

**Table 3**
LOI and UL-94 date of EVA/brucite, EVA/PM and EVA/CFR composites.

| Sample formulation | Composition (wt %) | | LOI | UL-94 |
|---|---|---|---|---|
| | EVA | FR | | |
| Virgin EVA | 100 | 0 | 17 | Fail |
| EVA/brucite | 60 | 40 | 22 | Fail |
| | 50 | 50 | 25 | Fail |
| | 40 | 60 | 35 | V-0 |
| EVA/PM | 60 | 40 | 28 | Fail |
| | 50 | 50 | 32 | V-0 |
| | 40 | 60 | 38 | V-0 |
| EVA/CFR | 60 | 40 | 32 | V-0 |
| | 50 | 50 | 35 | V-0 |
| | 40 | 60 | 39 | V-0 |

The most significance of brucite flame retardant is the absorption of smoke due to the formation of MgO layers in fire. The dynamic curves of smoke production rate (SPR) for the three EVA/FR blends were shown in Fig. 8. Owing to the reduction of specific surface area caused by the agglomeration of MgO particles (Fig. 10a), the SPR of sample A1 and A2 was much higher than that of sample A3. For instance, a remarkable increase of SPR peak value was observed from 0.012 $m^2/s$ of sample A3 to 0.036 $m^2/s$ of sample A1, which implied that the core/shell structure brought more advantages of dispersity of MgO in residue char, and could absorb more smoke by increasing specific surface area. Obviously, the above results further verified that excellent flame retardancy and smoke suppression were given by the core/shell structure of CFR.

The FESEM images of combustion residues from sample A1, A2 and A3 were shown in Fig. 10. It could be seen that the major

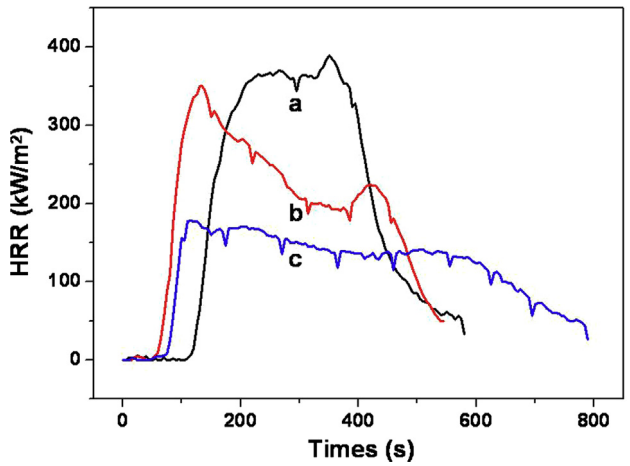


**Fig. 5.** HRR curves of (a) A1, (b) A2 and (c) A3.

structure of sample A1 and A2 almost collapsed because of the agglomeration of MgO particles (Fig. 10a and b) in the process of polymer composite burning. On the contrary, the residue of sample A3 (Fig. 10c, d, e and f) was more intact and compact, which maintained the original appearance to form an obvious fence structure with a remarkable expansion in volume (Fig. 9). This suggested that the internal released combustible gases and external heat could be prevented from passing through during burning. For PM additive, however, large cavities were observed on the surface of residue which might lead to promotion of heat and combustible gases transfer (Fig. 10b).

### 3.4. Flame retardant mechanism

The detailed mechanism on the enhanced flame resistance of the core/shell structure was proposed as Scheme 2. Accordance with the endothermic decomposition of brucite to MgO, the core of brucite played the role of mineral flame retardant in fire. More importantly, the shell of dodecylamine polyphosphate acted as the synergy agent in this system, which could result in dehydration of EVA to compact chars and form stable connection between MgO particles once fire occurred. In comparison with the collapse of chars layer (Fig. S3a), the intact and compact fence structure at EVA/CFR surface (Fig. S3b) was benefit for the reinforce of surface chars. When a large amount of these structures formed from the fire surface, the external heat radiation from burning area to the undegraded EVA would be barriered or slowed down. Without enough supplement of combustible gases in burning area, the combustion was difficult to maintain.

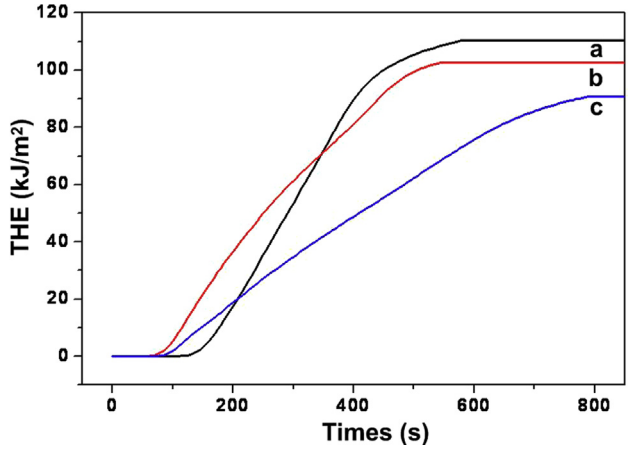


**Fig. 6.** THE curves of (a) A1, (b) A2 and (c) A3.

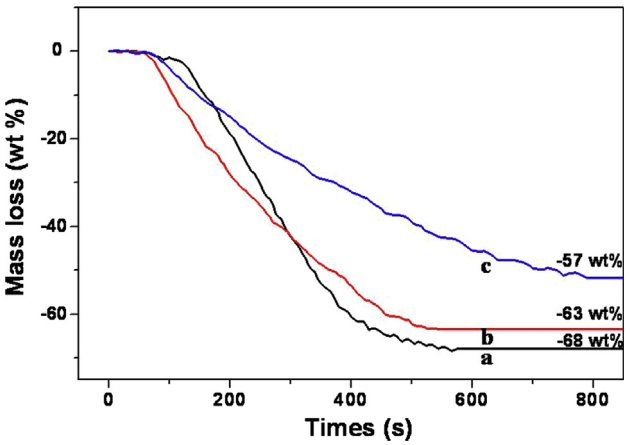


**Fig. 7.** Mass loss curves of (a) A1, (b) A2 and (c) A3.

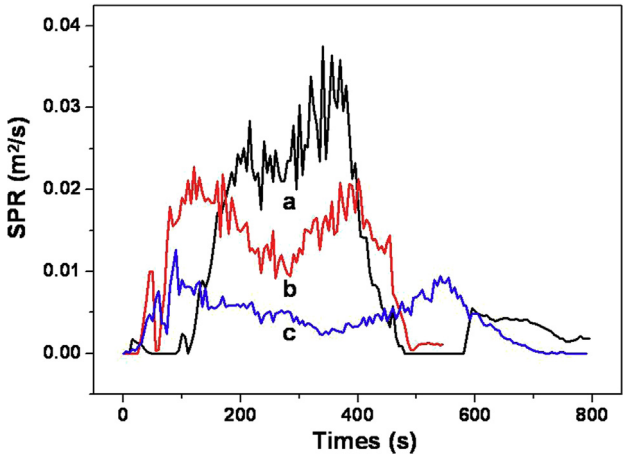


**Fig. 8.** SPR curves of (a) A1, (b) A2 and (c) A3.

## 4. Conclusions

In summary, a novel microsize flame retardant consisting of a brucite core and a dodecylamine polyphosphate shell has been

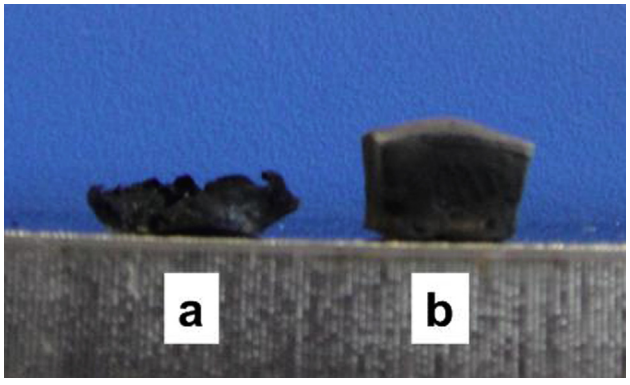


**Fig. 9.** Pictures of combustion residues: (a) EVA/brucite and (b) EVA/CFR composites.

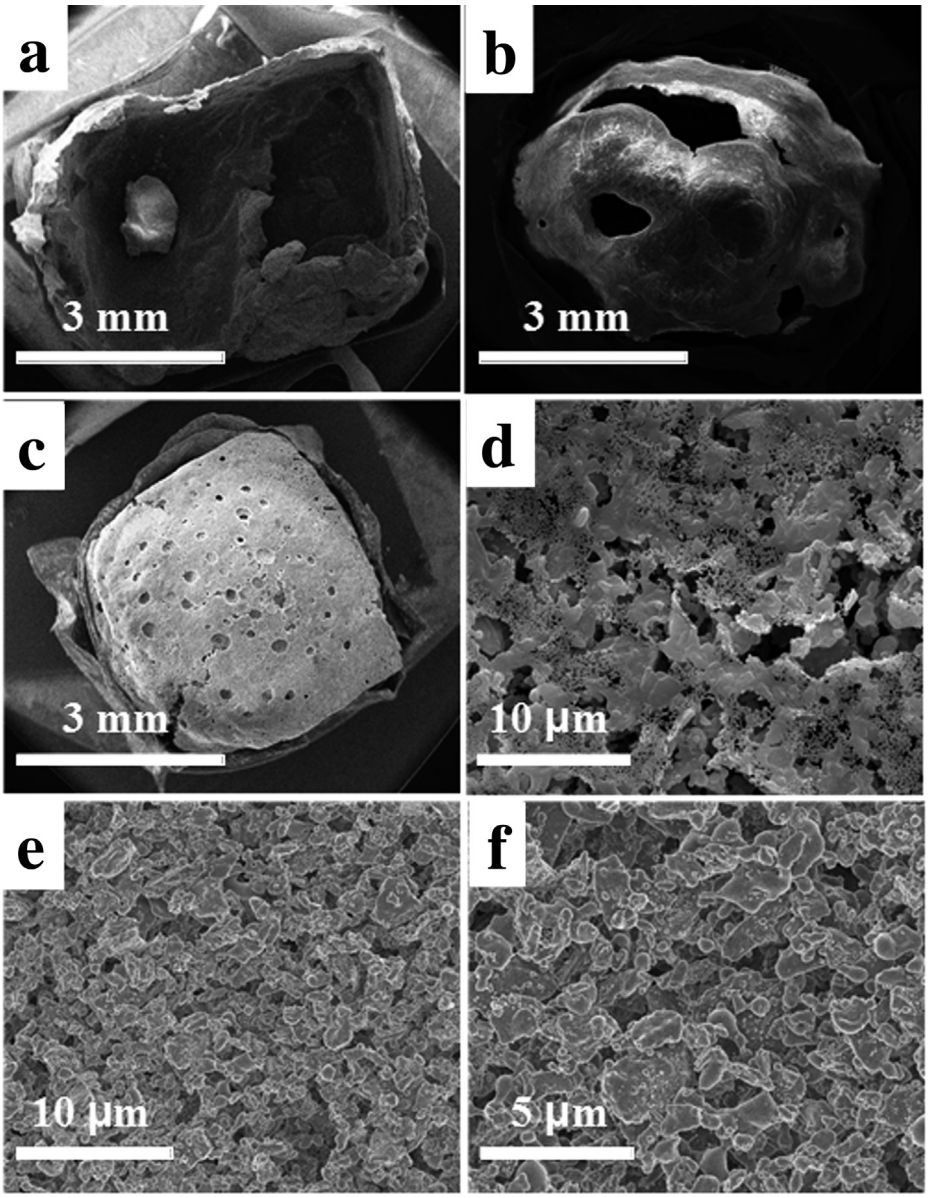


**Fig. 10.** FESEM images of combustion residues obtained by CONE alternative. (a) Low magnification views of sample A1. (b) Low magnification views of sample A2. (c) Low and (d) high magnification views of sample A3. (e) Low and (f) high magnification cross-sections of sample A3.

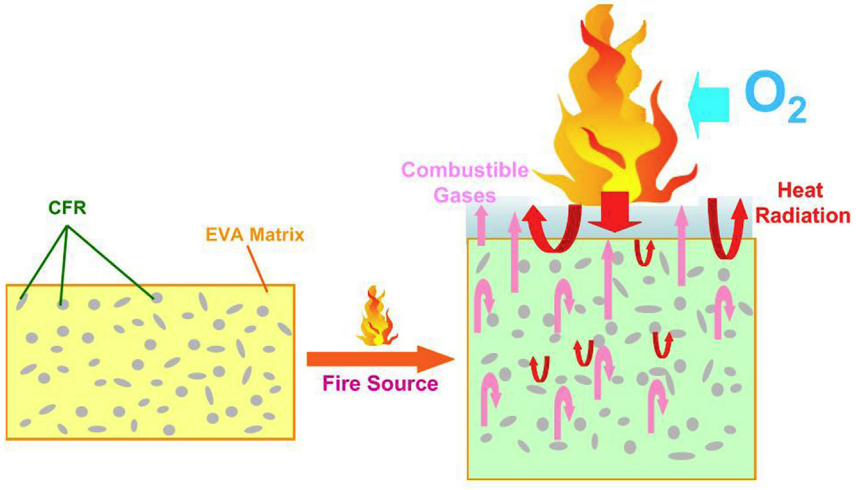


**Scheme 2.** A schematic illustration of the mechanism for the enhanced flame resistance of the core/shell structure.

synthesized by a two-step nanoengineering method. The core and the shell were connected by chemical attachment which could maintain a stable fence structure in fire. The polymer composite filled with core/shell flame retardant (CFR) exhibited unique flame resistance. Based on the massive evidence, the mechanism for the enhanced flame resistance of the core/shell structure was proposed. These results suggested the core/shell structure might be a promising design for mineral flame retardant application as green flame retardant.

## Acknowledgements

G. L. Ning and other authors thank the NSFC (Grant 21076041 and 21276046) for financial support and gratefully acknowledge the supporting characterization at Electron Microscope Lab, Dalian University of Technology.

## Appendix A. Supplementary data

Supplementary data related to this article can be found at http://dx.doi.org/10.1016/j.polymdegradstab.2013.09.021.

## References

[1] Rothon RN, Hornsby PR. Flame retardant effects of magnesium hydroxide. Polym Degrad Stab 1996;54(2–3):383–5.
[2] Yu JC, Xu AW, Zhang LZ, Song RQ, Wu L. Synthesis and characterization of porous magnesium hydroxide and oxide nanoplates. J Phys Chem B 2004;108(1):64–70.
[3] Pang HC, Ning GL, Gong WT, Ye JW, Lin Y. Direct synthesis of hexagonal $Mg(OH)_2$ nanoplates from natural brucite without dissolution procedure. Chem Commun 2011;47:6317–9.
[4] Montezin F, Lopez-Cuesta JM, Crespy A, Georlette P. Flame retardant and mechanical properties of a copolymer PP/PE containing brominated compounds/antimony trioxide blends and magnesium hydroxide or talc. Fire Mater 1997;21(6):245–52.
[5] Giorgi R, Bozzi C, Dei L, Gabbiani C, Ninham BW, Baglion P. Nanoparticles of $Mg(OH)_2$: synthesis and application to paper conservation. Langmuir 2005;21(18):8495–501.
[6] Durin-France A, Ferry L, Lopez-Cuesta JM, Crespy A. Magnesium hydroxide/zinc borate/talc compositions as flame-retardants in EVA copolymer. Polym Int 2000;49(10):1101–5.
[7] Hornsby PR, Cusack PA, Cross M, Toth A, Zelei B, Marosi G. Zhs-coated metal hydroxide flame retardants: fire performance and substrate coating interation. J Mater Sci 2003;38:2893–9.
[8] Cross MS, Cusack PA, Hornsby PR. Effects of tin additives on the flammability and smoke emission characteristics of halogen-free ethylene-vinyl acetate copolymer. Polym Degrad Stab 2003;79(2):309–18.
[9] Carpentier F, Bourbigot S, Bras ML, Delobel R, Foulon M. Charring of fire retarded ethylene vinyl acetate copolymer-magnesium hydroxide/zinc borate formulations. Polym Degrad Stab 2000;69(1):83–92.
[10] Li X, Ye JW, Lin Y, Fan LL, Ning GL. Synergistic flame retarded effect of synthetic dawsonite on EVA/magnesium hydroxide system. Polym Plast Technol 2010;49:861–86.
[11] Xie RC, Qu BJ. Expandable graphite systems for halogen-free flame-retarding of polyolefins. I. Flammability characterization and synergistic effect. J Appl Polym Sci 2001;80(8):1181–9.
[12] Fu MZ, Qu BJ. Synergistic flame retardant mechanism of fumed silica in ethylene-vinyl acetate/magnesium hydroxide blends. Polym Degrad Stab 2004;85(1):633–9.
[13] Bourbigot S, Bras ML, Leeuwendal R, Shen KK, Schubert D. Recent advances in the use of zinc borates in flame retardancy of EVA. Polym Degrad Stab 1999;64(3):419–25.
[14] Wang ZZ, Qu BJ, Fan WC, Huang P. Combustion characteristics of halogen-free flame-retarded polyethylene containing magnesium hydroxide and some synergists. J Appl Polym Sci 2001;81(1):206–14.
[15] Liu SP, Ying JR, Zhou XP, Xie XL, Mai YW. Dispersion, thermal and mechanical properties of polypropylene/magnesium hydroxide nanocomposites compatibilized by SEBS-g-MA. Compos Sci Technol 2009;69(11–12):1873–9.
[16] Chang SQ, Xie TX, Yang GS. Effects of polystyrene-encapsulated magnesium hydroxide on rheological and flame-retarding properties of HIPS composites. Polym Degrad Stab 2006;91(12):3266–73.
[17] Chang SQ, Xie TX, Yang GS. Effects of shell thickness of polystyrene-encapsulated $Mg(OH)_2$ on flammability and rheological properties of high-impact polystyrene composites. Polym Int 2007;56(9):1135–41.
[18] Salaun F, Vroman I, Bedek G, Lewandowski M. Effects of microparticles on isotactic polypropylene: thermomechanical and thermal properties. Polym Sci Part B Polym Phys 2008;46(23):2566–76.
[19] Taguchi Y, Takahashi M, Tanaka M. Microencapsulation of hydrophilic solid powder as a fire retardant by the method of in situ gelation in droplets using a non-aqueous solvent as the continuous phase. Polym Polym Compos 2009;17(2):83–90.
[20] Luo WJ, Yang W, Jiang S. Microencapsulation of decabromodiphenyl ether by in situ polymerization: preparation and characterization. Polym Degrad Stab 2007;92(7):1359–64.
[21] Lin M, Yang Y, Xi P, Chen SL, et al. Microencapsulation of water-soluble flame retardant containing organophosphorus and its application on fabric. J Appl Polym Sci 2006;102(5):4915–20.
[22] Chang SQ, Xie TX, Yang GS. Effects of interfacial modification on the thermal, mechanical, and fire properties of high-impact polystyrene/microencapsulated red phosphorous. J Appl Polym Sci 2008;110(4):2139–44.
[23] Liu Y, Wang Q. Preparation of microencapsulated red phosphorus through melamine cyanurate self-assembly and its performance in flame retardant polyamide 6. Polym Eng Sci 2006;46(11):1548–53.
[24] Wang XS, Ye JW, Pang HC, Gong WT, Lin Y, Ning GL. Preparation and application of brucite matrix organic-inorganic composite flame retardant. Chin J Funct Mater 2010;12:2124–7.
[25] Leonard JE, Bowditch PA, Dowling VP. Development of a controlled-atmosphere cone calorimeter. Fire Mater 2000;24(3):143–50.
[26] Weil ED, Hirschler MM, Patel NG, Said MM, Shakir S. Oxygen index: correlations to other fire tests. Fire Mater 1992;16(4):159–67.
[27] Hirschler MM. How to measure smoke obscuration in a manner relevant to fire hazard assessment: use of heat release calorimetry test equipment. J Fire Sci 1991;9(3):183–222.
[28] Yan H, Zhang XH, Wei LQ, Liu XG, Xu BS. Hydrophobic magnesium hydroxide nanoparticles via oleic acid and poly(methyl methacrylate)-grafting surface modification. Powder Technol 2009;193(2):125–9.
[29] Liauw CM, Rothon RN, Lee GC, Iqbal Z. Flow micro-calorimetry and FTIR studies on the adsorption of saturated and unsaturated carboxylic acids onto metal hydroxide flame-retardant fillers. J Adhes Sci Technol 2001;15:889–912.
[30] Li HY, Wang RG, Hu HL, Liu WB. Surface modification of self-healing poly(-urea-formaldehyde) microcapsules using silane-coupling agent. Appl Surf Sci 2008;255(5):1894–900.
[31] Haworth B, Raymond CL, Sutherl I. Polyethylene compounds containing mineral fillers modified by acid coatings. 1: characterization and processing. Polym Eng Sci 2000;40(9):1953–68.
[32] Isitman NA, Gunduz HO, Kaynak C. Nanoclay synergy in flame retarded/glass fibre reinforced polyamide 6. Polym Degrad Stab 2009;94(12):2241–50.
[33] Balakrishnan H, Hassan A, Isitman NA, Kaynak C. On the use of magnesium hydroxide towards halogen-free flame-retarded polyamide-6/polypropylene blends. Polym Degrad Stab 2012;97:1447–57.